Influence of Particle Size Distribution on Lifetime and Thermal Stability of Ostwald Ripening of Supported Particles

Sulei Hu[a, d] and Wei-Xue Li*[a, b, c]

Stability of dispersed particles on their supports is one of the central topics in heterogeneous catalysis and quantifying the influence of the particle size distribution on lifetime and thermal stability is highly valuable for rational design of efficient nanocatalysts. We report here a theoretical study of Ostwald ripening of supported particles, in particular, the kinetic evolution of particle number, average size, and dispersion with respect to time and thermal temperature in a wide range of size and monodispersity. Phase diagrams of half-lifetime and onset temperature of ripening as functions of size and monodispersity were constructed. If decreasing the average particle size, though there is a modest gain in the dispersion, the stability declines dramatically; specifically, the half-lifetime of ripening decreases exponentially and the corresponding onset temperature decreases by hundreds of Kelvin. Decline in stability owing to the decrease in size could, however, be systematically compensated by increasing the monodispersity of the size distribution. We find that the supported particles with the same half-life time and onset temperature could originate from different particle size distributions, whereas the particle size distribution with the same apparent dispersion could have very different onset temperature and half-lifetime. The result highlights the importance of both size and monodispersity in particle size distribution to the ripening resistance of supported particles, and the methodology developed for simulating ripening kinetics could be used to accelerate the aging protocols.

Introduction

Supported transition metals are often prepared in small size (typically in nanometers) for high surface area, dispersion, and low coordination sites with potentially higher activity and selectivity.[1] However, high surface free energy at small size dramatically destabilizes the corresponding particles,[2] which would eventually grow and sinter towards the large ones via particle migration and coalescence (PMC)[3] and/or Ostwald ripening (OR).[4] For sintering of supported particles, the average size increases gradually with time and thermal temperature, accompanied by a decrease of dispersion, surface area, and particle number.[5] This in turn influences the activity, selectivity, and stability of supported catalysts.[6] However, sintering kinetics are complicated and depend sensitively on metal–support interaction,[7] metal–reactant interaction,[4d, 8] and particle spatial and size distribution.[4e, 9] Identifying their influences on corresponding lifetime and thermal resistance of the supported particles are crucial for the industrialization of laboratory catalysts and commercialization of nanomaterials in general.

We present here a theoretical study on Ostwald ripening of supported particles and the influence of the particle size distribution (PSD) on the ripening resistance. Ostwald ripening proceeds through the growth of the larger particles at the expense of the smaller ones owing to the gradient difference of monomer concentration between supported particles, and a detailed description of corresponding rate equation can be found in the literature[4b] and references therein. Though smaller particles would disappear faster and at lower temperature than larger ones,[5b,c] it is unknown yet how the particle size affects quantitatively the durability of catalysts, which is very important to balance the surface area and the stability of the catalysts for practical application.[6a, 10] In this context, not only the lifetime under isothermal condition but more importantly the thermal stability as resistance to temperature are concerned and will be addressed in the present work.

[a] S. Hu, Prof. W.-X. Li
State Key Laboratory of Catalysis
Dalian Institute of Chemical Physics
Chinese Academy of Sciences
Dalian 116023 (P.R. China)

[b] Prof. W.-X. Li
Department of Chemical Physics
School of Chemistry and Materials Science, iCHeM, CAS Excellence Center for Nanoscience
University of Science and Technology of China
Hefei 230026 (P.R. China)
E-mail: wxli70@ustc.edu.cn

[c] Prof. W.-X. Li
Hefei National Laboratory for Physical Sciences at the Microscale
University of Science and Technology of China
Hefei 230026 (P.R. China)

[d] S. Hu
University of Chinese Academy of Sciences
Chinese Academy of Sciences
Beijing 100049 (P.R. China)

For decades, supported particles with monodisperse distribution and narrow size distribution were used to simplify the investigations of structure–activity relationship and facilitate the functionalization of nanodevices.[11] Based on thermodynamics analysis, we predicted that the size monodispersity could also efficiently suppress the ripening by diminishing the gradient difference of monomers between supported particles.[12] The prediction was confirmed by subsequent experiments and Monte Carlo simulation,[13] though fluctuation could deviate the system from the ideal monodispersity.[14] Recent experimental study further showed that the use of monodispersed nanoparticles could help to differentiate the relative contribution of OR and PMC to the overall growth process,[15] which is important for mechanistic understanding of sintering process. Nevertheless, how the monodispersity influences quantitatively the lifetime and the thermal stability of supported particles has remained to be explored. It is also unclear how monodispersity and particle size interplay with each other and affects the overall ripening kinetics. Quantitative investigations on these are important since it adds an effective way to improve the stability of supported particles, in addition to optimize for instance the metal-support interaction.

In this work, the influence of size and monodispersity on the ripening kinetics of supported particles was addressed through kinetic simulation, whereas the influence of metal–support interaction and metal–reactant interaction on the ripening kinetics of supported particles was represented in our recent works.[16, 17] Herein, we present a detail evolution of dispersion, average size, and particle number for Ostwald ripening of supported particles under both isothermal and thermal conditions, from which corresponding half-lifetime and onset temperature were extracted to quantify the lifetime and thermal stability. Accordingly, the phase-diagrams of half-lifetime and onset temperature over a wide range of size and monodispersity are constructed for the first time. The interplay between size and monodispersity as well as the implication of the apparent dispersion on the overall stability of supported particles will be highlighted.

Results and Discussion

Isothermal and temperature-programmed aging

First, we investigated the ripening kinetics under isothermal condition. The initial PSD, a normalized Gaussian distribution with the average particle diameter $<d_0> = 3$ nm and the relative standard deviation $rsd = 10\%$, is plotted in Figure 1. Under isothermal condition of 800 K, the PSD peak shifts toward the larger diameter with time, and corresponding peak height decreases. This shows typically how the ripening kinetic evolves: growth of the larger particles with expense of the smaller ones, and accordingly the average size increases, the particle number decreases. Moreover (Figure 2b), the PSD shape changes gradually from a Gaussian-type distribution to Lifshitz–Slyozov–Wagner (LSW) type distribution with a long tail toward the small particles. Meanwhile, during the ripening
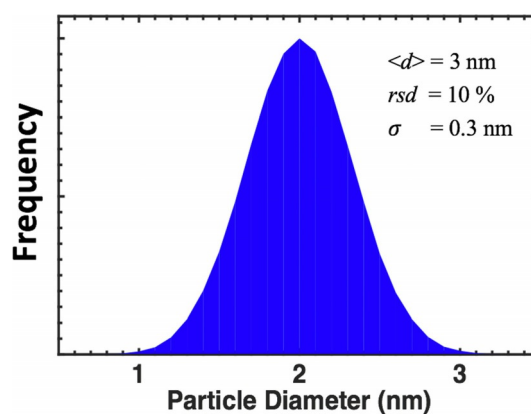

Figure 1. Gaussian-like particle size distribution. Average particle diameter $<d> = 3$ nm, standard deviation $\sigma = 0.3$ nm, relative standard deviation $rsd = 10\%$.
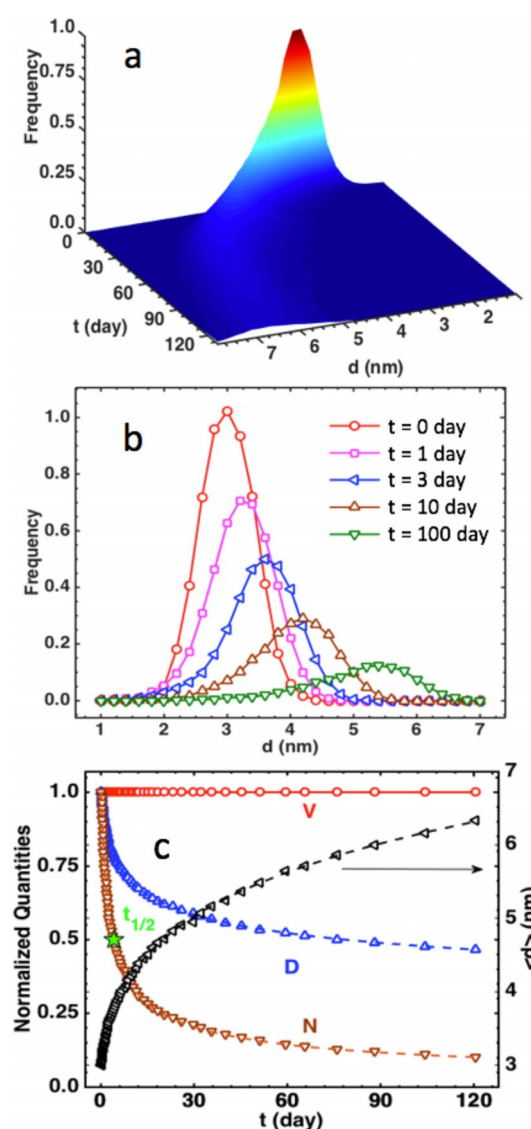

Figure 2. (a) Evolution of particle size distribution under isothermal temperature of 800 K, and (b) snapshots at different times. (c) Evolution of the normalized volume V (circle), dispersion D (triangle) and particle number N (inverted triangle), and average diameter $<d>$. Half-lifetime $t_{1/2}$ (star) is indicated.

(Figure 2c), the total volume (or mass) is conserved, validating the algorithm implemented.

From the above results, the evolution of the particle number N, dispersion D (the ratio between surface and total atom number of supported particles), and average size $<d>$, can be derived as plotted in Figure 2c. For convenience, N and D at $t=0$ are normalized to one throughout the present work. It can be found that the dispersion first drops steeply, and then decreases smoothly afterward. This is understandable because at the earlier stage of ripening, there are more small particles with a higher chemical potential, and the driving force for ripening is high. A similar trend variation is found for the evolution of the particle number as well, but the extent of variation is larger. In line with this change, the average size increases gradually.

Ripening rate is sensitive to temperature, and may increase rapidly with increase of T. To quantify its dependence, we studied the ripening under temperature-programmed aging (TPA) condition. A typical result starting from 200 K with a heating rate of $1\,K\,s^{-1}$ is plotted in Figure 3a. When T is lower than 900 K, there is nearly nothing change in PSD shape as well as N, D and $<d>$. This can be rationalized by large total activation energy of 3 eV used in present work, and influence of total activation energy on ripening kinetics can be found in our recent work.[16] When temperature is heated up to 935 K, there is about 11% decrease of the peak height and 0.26 Å right shift of peak position (Figure 3b). After this, the ripening proceeds faster. The resulting PSD remains LSW-like, same with isothermal condition. As shown in Figure 3c, N and D decay nearly linearly with T. Namely, there is no decrease of the ripening slope with respect to the ramping temperature, in contrast to the isothermal ripening. This tells us that the increase of the ripening rate with the ramping temperature overwhelms the decrease of the ripening rate due to the increase of size. This illustrates the large influence of the temperature on ripening.

To quantify the ripening resistance below, two characteristic variables are defined. For isothermal ripening, it is the half-life-time $t_{1/2}$, the time expended for half decrease of the particle number N (Figure 2c). In contrast, for the ripening under TPA, it is the onset temperature T_{on}, namely, the temperature raised for a ten percent decrease of N (Figure 3c). We note that using the particle number rather than the dispersion and/or average size to evaluate the ripening resistance is simply because of its sensitivity with time and temperature. Using the evolution of dispersion and/or average size to evaluate the ripening resistance gives essentially the same trend behavior.

Half-lifetime and onset temperature of ripening

To study the influence of size and monodispersity on half-life-time and onset temperature, the ripening kinetics of supported particles at a wide range of average size and monodispersity are studied. Again, a heating rate of $1\,K\,s^{-1}$ starting from 200 K for TPA and an isothermal temperature of 800 K for isothermal condition are used throughout the present work unless stated otherwise. First, initial PSDs for $<d_0>=1$, 3, and 5 nm at given of $rsd=10\%$ are plotted in Figure 4a, and corre-
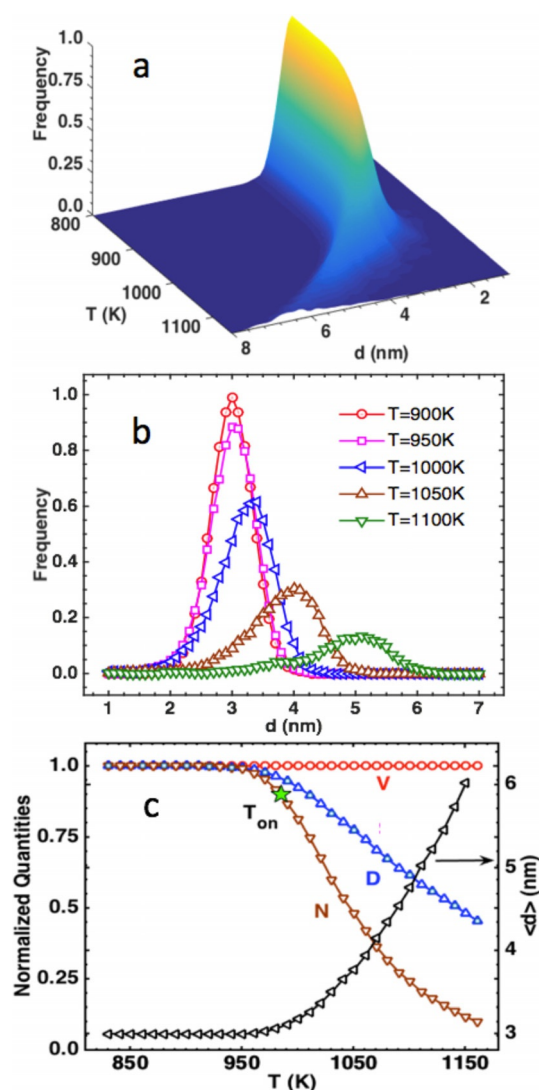

Figure 3. (a) Evolution of particle size distribution under ramping temperature at a heating rate of $1\,K\,s^{-1}$ and starting from 200 K, and only plotting the result if notable change observed. (b) Snapshot at different ramping temperature. (c) Evolution of the normalized volume V (circle), dispersion D (triangle), and particle number N (inverted triangle), and average diameter $<d>$ in right y-axis. Onset temperature T_{on} (star) is indicated.

sponding evolution curves of particle number N with temperature and time are plotted in Figure 4b and 4c, respectively. For PSD with a larger $<d_0>$ of 5 nm, calculated $t_{1/2}$ and T_{on} are 2863 d and 1160 K, respectively. If decreasing the size by 2 nm ($<d_0>=3$ nm), corresponding $t_{1/2}$ decreases by a factor of fifteen (186 d), and T_{on} lowers by 91 K (1072 K). It is clear that the ripening starts at a earlier time and ignites at a lower temperature with decrease of size; namely, the smaller the size, the poorer the ripening resistance. By further decreasing the size by another 2 nm to $<d_0>=1$ nm, the corresponding T_{on} lowers by 195 K to 877 K, and $t_{1/2}$ decreases by three orders of magnitude to 0.15 d. In other words, the decline of the ripening resistance increases rapidly with decrease of the size.

The plots in Figure 5 show the dependence of T_{on} and $t_{1/2}$ on the size. Both $t_{1/2}$ and T_{on} are monotonic functions of the size and decrease faster with size decreasing. The dramatic decline
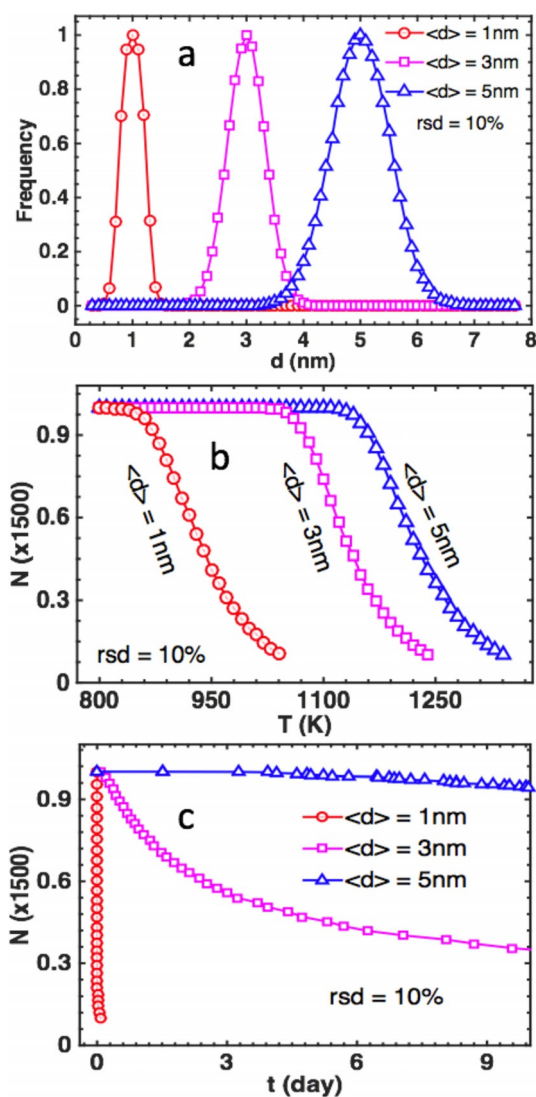
Figure 4. Particle size distribution for different (a) $<d_0> = 1$, 3 and 5 nm ($rsd = 10\%$) and (b) evolution of corresponding particle number with respect to the ramping temperature and (c) time under isothermal condition of 800 K under the same $rsd = 10\%$.

Figure 5. (a) Onset temperature T_{on} (K) and (b) half-lifetime $t_{1/2}$ (day in logarithm) versus different initial average particle diameter $<d>$ under the same relative standard deviation $rsd = 10\%$.

of the ripening resistance at small size can be rationalized by the higher chemical potential of the smaller particle and the fact that the ripening rate [Eq. (1)] is proportional to the inverse of the square of the curvature radius. We note that decreasing $<d_0>$ from 5 to 1 nm only increases the dispersion by a factor of five. Assuming the catalytic reaction is structural insensitive, and the mass-specific activity is proportional to dispersion, the mass specific activity would increase by a factor of five as well. However, as shown above, the corresponding onset temperature and half-lifetime for ripening will decrease by 286 K and four orders of magnitude, respectively. This indicates that the decline of the stability with decrease in size is far more severe than the gain in dispersion and possible mass-specific activity. Even for structure-sensitive reactions, which may have higher intrinsic activity at small size, the dramatic decrease in stability remains a crucial issue.

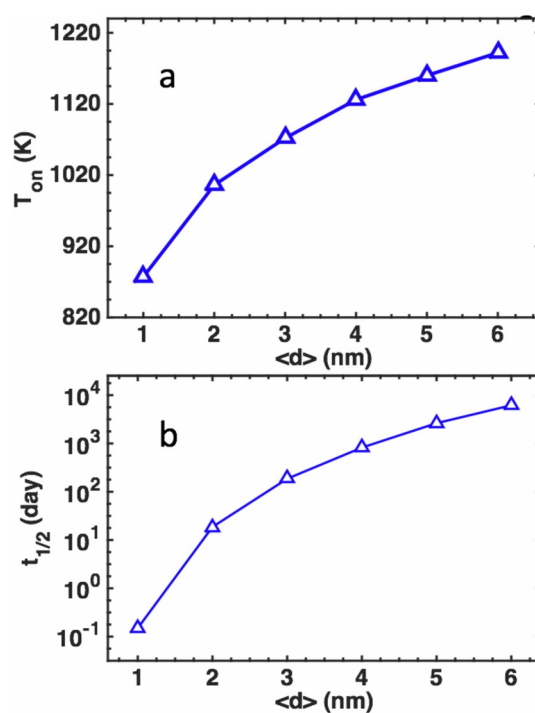Influence of the monodispersity on the ripening resistance is studied by considering PSDs with different rsd varying from 1, 10, and 30% at given $<d_0>$ of 2 nm (Figure 6a). We note that the smaller the rsd, the higher the monodispersity. Corresponding evolution curves of the particle number with ramping temperature and time are plotted in Figure 6b and 6c, respectively. It can be found that with a gradual decrease of rsd, ripening occurs at higher temperature and later time. Namely, the higher the monodispersity, the better the ripening resistance. To see this more clearly, we plot the calculated T_{on} and $t_{1/2}$ at a wide range of rsd varying from 10^{-3} to 50% in Figure 7. For the PSD with the poorest monodispersity considered ($rsd = 50\%$), the corresponding T_{on} and $t_{1/2}$ are 936 K and 10 d. With increase of the monodispersity, both T_{on} and $t_{1/2}$ increase monotonically. For the PSD with the highest monodispersity considered ($rsd = 10^{-3}\%$), corresponding T_{on} and $t_{1/2}$ are 1102 K and 50 000 d, respectively. Compared to the result of $rsd = 50\%$, T_{on} and $t_{1/2}$ increase by 166 K and 5000 times, respectively, a fact that may compensate considerably the loss of the ripening resistance due to the decrease in size. This provides a promising perspective about the monodispersity on improving the ripening resistance, which is especially important for the smaller particles.

We note that for small rsd of 1%, there is nearly no observable change for the particle number in a considerable range of time and/or temperature (Figure 6b). Only once the time is longer than a threshold time, noted as the residence time t_0, the ripening takes place. For PSD with rsd of 1%, the corresponding t_0 is approximately 24 d, contributing about half of $t_{1/2}$ (48 d). For PSD with poorer monodispersity, it decreases rapidly and becomes for instance 0.2 d at $rsd = 30\%$, though corresponding half-lifetime remains considerable 10 d. For the
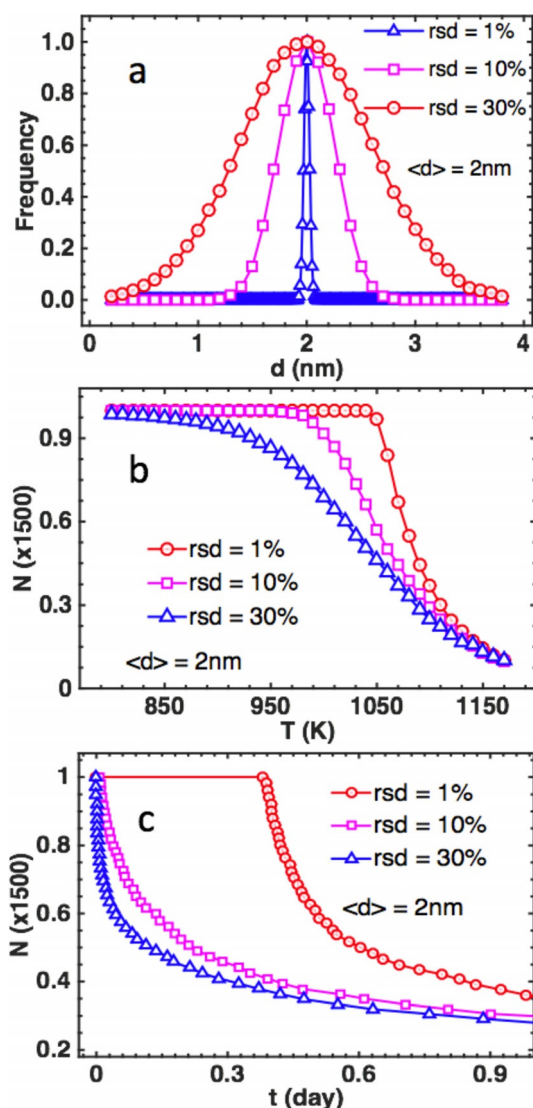
Figure 6. Particle size distribution for different (a) $rsd = 1\%$, 10% and 30% and evolution of particle number with (b) ramping temperature and (c) time under isothermal condition of 800 K under the same initial $<d> = 2$nm.

Figure 7. (a) Onset temperature T_{on} (K) and (b) half-lifetime $t_{1/2}$ (day in logarithm) versus relative standard deviation rsd under the same initial $<d> = 2$ nm.

bution, and deviates eventually the ideal monodispersity.[14] In reality, there are even more uncontrolled issues preventing or breaking the ideal monodispersity, for instance, inhomogeneity in spatial distribution, support heterogeneity, and distinct metal–support interfaces. Nevertheless, there are growing efforts to improve monodispersity and homogeneity, for instance by mass-selected cluster technique[13, 18] or digestive ripening.[19] In addition, a negative effective surface energy by surface passivation, i.e., using ligands binding strongly with the particle surfaces, provides a possible mechanism to stabilize the monodispersed size distribution as well.[20]

PSD with higher monodispersity, it increases rapidly and becomes 6230 d at $rsd = 10^{-2}$%, which contributes to the most part of the half-lifetime ($t_{1/2} = 6620$ d). This tells us that the residence time becomes considerable only for a reasonable good monodispersity, and it increases quickly with monodispersity and soon becomes decisive for the overall ripening resistance.

The above results can be rationalized from the ripening rate equation. For the PSD with ideal monodispersity, all particles have the same chemical potential, and each particle has the same R and equals to the critical radius of R^*. The gradient difference of the far-field monomer between the supported particles becomes zero, and there is neither increase nor decrease in the net mass for each particle. As a result, all the particles fall in a quasi-stationary state, and the ripening resistance increases accordingly. In this context, we note that recent Monte Carlo simulation indicated that fluctuation in the monomer detachment and attachment rates might broaden the size distri-
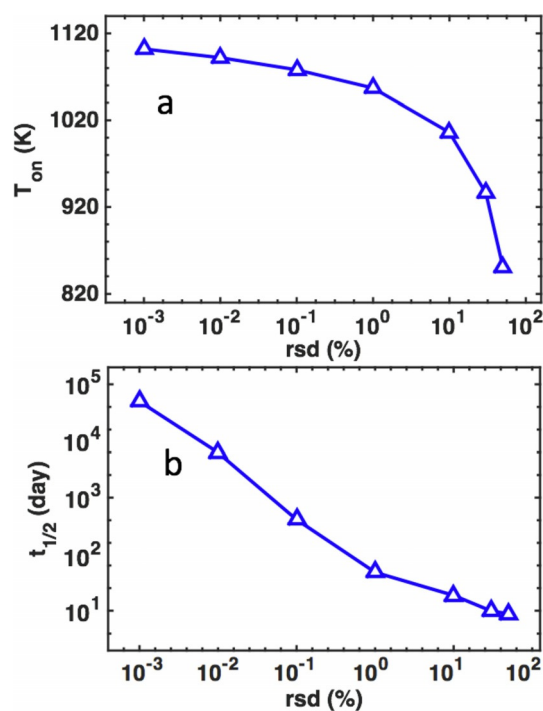
Dispersion and particle size distribution

The dispersion of supported particles increases inversely proportional to the size considering more atoms are exposed. On the other hand, dispersion is also a function of monodispersity. For instance, if rsd increases from 1 to 10 to 30% at $<d_0> = 2$ nm, the corresponding dispersion decreases from 49.9 to 43.7 to 36.7%. Actually, the effective dispersion increases with the inverse of rsd or monodispersity. This is understandable because the higher the monodispersity or the smaller the rsd, the less the amount of the larger particles with lower dispersion in PSD. As dispersion becomes a function of both size and monodispersity, different PSD might result in the same overall dispersion. For instance, the same dispersion of 17.6% can be realized for instance by a PSD with $<d_0> = 4.4$ nm and $rsd = 45$% but also by a PSD with a larger $<d_0> = 5.8$ nm and a smaller $rsd = 5$%. In other words, supported particles with a larger average size and higher monodispersity could have the

same dispersion as those with a smaller average size and lower monodispersity. To better visualize this, a two-dimensional contour of the dispersion with respect to the average size and monodispersity is plotted in Figure 8a. It is clear that high dispersion occurs at the left-bottom corner, having smaller size and higher monodispersity.

Since the ripening resistance depends on both size and monodispersity, supported particles with the same apparent dispersion but different size and monodispersity will have very different ripening resistance. For a PSD with $<d_0> = 2.2$ nm and $rsd = 45\%$, corresponding dispersion is 34.7%, and calculated T_{on} and $t_{1/2}$ are 867 K and 10 d, respectively. In contrast, for the PSD with the same apparent dispersion but different $<d_0>$ and rsd (2.9 nm and 8.9%), calculated T_{on} and $t_{1/2}$ are 1091 K and 219 d, respectively. Differences by 224 K for T_{on} and 22 times for $t_{1/2}$ show the significant influence of the PSD
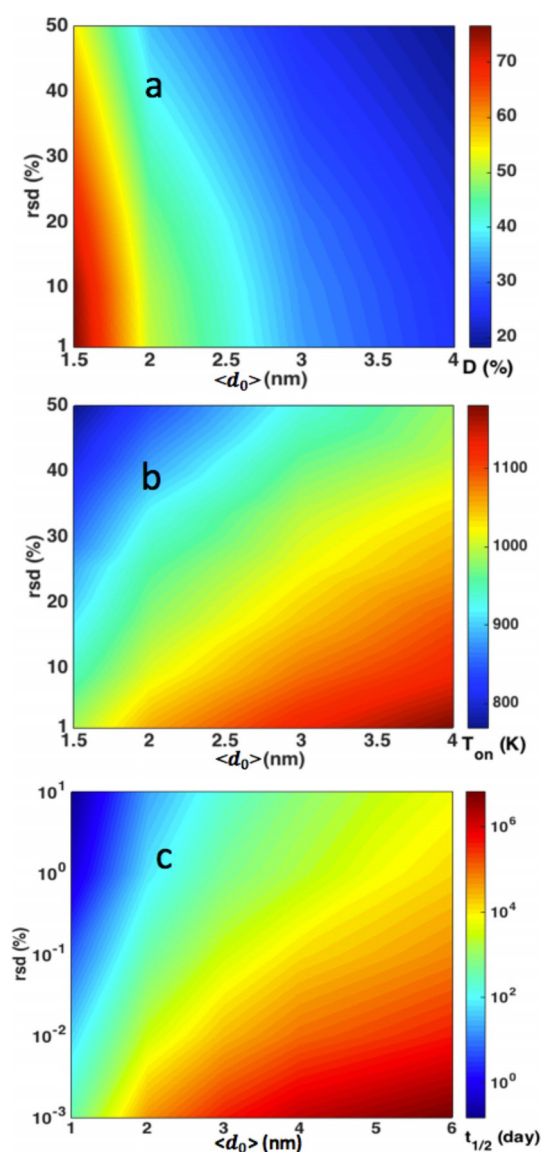
shape (average size and monodispersity) on the ripening resistance, though they have the same apparent dispersion.

The above results show that the dispersion alone cannot properly describe the ripening resistance. To describe the ripening resistance of supported particles, both the average size and monodispersity are required. Figure 8b and 8c are 2D contour plots of T_{on} and $t_{1/2}$ at a wide range of size and monodispersity. The poorest ripening resistance in Figure 8b and 8c is a PSD with small $<d_0>$ of 1.5 nm and large rsd of 50%, and corresponding T_{on} and $t_{1/2}$ are 769 K and 16 h. The best ripening resistance can be found for the PSD with large $<d_0>$ and small rsd of 6 nm and 10^{-3}%, and corresponding T_{on} and $t_{1/2}$ can be as high as 1255 K and 6.37×10^6 d.

Supported particles with different size and monodispersity might have the same onset temperature and half-lifetime. This can be seen from the contour lines plotted in Figure 8b and 8c as well. Specifically, for the PSD with small $<d_0>$ of 2.2 nm and rsd of 5%, corresponding T_{on} is 1050 K. While the PSD with large $<d_0>$ of 5.8 nm and rsd of 45% (not included in Figure) have exactly same T_{on}. This is because the gain in the ripening resistance due to increase of the size is largely counteracted by its poor monodispersity. Since T_{on} and $t_{1/2}$ describe earlier and middle stage of the ripening process, respectively, two PSDs with the same T_{on} do not necessarily have the same $t_{1/2}$. Actually, they could be very different, and corresponding $t_{1/2}$ of above mentioned two PSDs are 45 and 1905 d. It is also true that two PSDs with same $t_{1/2}$ can have different T_{on}. The fact that the supported particles with the same onset temperature and half-lifetime can originate from different PSDs, and those with the same apparent dispersion can have different onset temperature and half-lifetime, provides valuable insights on the interplay between PSD and dispersion as well as their influences on the ripening resistance.

We note that the present work focuses on the influence of PSD on ripening kinetics only. In addition, the metal–support interaction and metal–reactant interaction can affect significantly the corresponding kinetics, as shown in our recent works.[16,17] To describe the overall behavior of the ripening resistance and quantify their relative contributions, it is important to describe all of them consistently in one framework and corresponding work is ongoing.

Conclusions

Ostwald ripening for supported particles under both isothermal and temperature-programmed aging conditions was studied by solving the corresponding rate equation via an adaptive time step algorithm. Evolution of dispersion, average size, and particle number were explored at a wide range of size and monodispersity. Corresponding two-dimensional phase diagrams of the half-lifetime and thermal stability (onset temperature) were constructed.

It is found that though the dispersion of supported particles increases inversely proportional to the size, corresponding half-lifetime decreases exponentially in orders of magnitude, and onset temperature decreases dramatically by hundreds of Kelvin. The great difference between the modest gain in dis-

Figure 8. Two-dimensional plot (a) dispersion D as a function of initial average size $<d_0>$ and monodispersity rsd, the corresponding (b) onset temperature T_{on} (K) and (c) half-life $t_{1/2}$ (day in logarithm).

persion and severe decline in ripening resistance due to decrease in size requires stringently optimization of supports to stabilize corresponding particles. Nevertheless, our calculations find that the half-lifetime and thermal stability of ripening can be systematically improved by a gradual increase of the monodispersity. It could eventually compensate in a large extent the loss of stability owing to the decrease in size. It is therefore vital to synthesize nanocatalysts with single size distribution. For ideal monodispersion, one should further minimize the inhomogeneity of the particle spatial distribution and support.

The supported particles with the same apparent dispersion do not necessarily have the same lifetime and thermal stability unless they have exactly same particle size distribution, whereas the supported particles with the same onset temperature and half-lifetime could originate from very different particle size distributions. Moreover, the supported particles with high dispersion could be rather stable if having high monodispersity. It is the average size and the monodispersity together, in addition to the metal–support interaction and metal-reactant interaction, determining the overall lifetime and thermal stability of supported particles. Finally, the approach implemented is expected useful for the design of practical catalysts, given specific material properties and predetermined temperature ranges and catalysts target lifetime. It could also be applied for the design and validation of accelerated aging protocols.

Ripening Kinetic Model and Algorithm

Rate equation for Ostwald ripening of supported particles can be found in previous works (references therein),[4b, 12] and the key points are given here for convenience. Under the steady state, the evolution of particle at a given curvature radius R follows the rate equation below [Eq. (1)]:

$$\frac{dR}{dt} = \frac{XY}{X+Y} \frac{K}{R^2} \left(\exp\left[\frac{\Delta\mu(R^*)}{\kappa_B T}\right] - \exp\left[\frac{\Delta\mu(R)}{\kappa_B T}\right] \right) \exp\left[-\frac{E_{tot}}{\kappa_B T}\right] \quad (1)$$

where K, X, and Y are a function of R, diffusion length L of the monomer, contact angle α between particle and support. E_{tot} is the total activation energy of ripening process, decided by the summation of formation energy of monomer (or metal-reactant complexes) and corresponding diffusion barrier on supports. Chemical potential $\Delta\mu(R)$ of atom in supported particles with respect to bulk counterpart is approximated here by Gibbs–Thomson (GT) relation [Eq. (2)]

$$\Delta\mu(R) = \frac{2\Omega\gamma}{R} \quad (2)$$

where Ω is the molar volume of bulk metal atom, and γ is the surface free energy of supported particles. We note that for small particle, γ might be size dependent due to the increasing ratio of the low coordination sites.[21] Experimentally, the projection diameter d of the particle is conveniently extracted from experiment. To substitute R with d in above rate equation, we should consider the follows relationship: when $0 < \alpha \leq \pi/2$, $d = 2R\sin(\alpha)$, and when $\pi/2 \leq \alpha \leq \pi$, $d = 2R$, assuming particle in a spherical segment morphology. Accordingly, the influence of supports was taken into account. The GT-like relation taking into account of supports was reported recently.[22] As we focus on the influence of particle size dis-

tribution on the ripening kinetics, for simplicity surface energy and contact angle were assumed constant. Specifically, $E_{tot} = 3$ eV, $\alpha = 90°$ and $\gamma = 94$ meV Å^{-2} are used in the present work.

For supported particles, corresponding initial particle size distribution (PSD) function $f(R, t)$ is assumed to follow a Gaussian-like distribution (Figure 1). We are interesting here in the influence of average size $<d> = 2<R>$ and monodispersity, namely, standard deviation σ (the relative standard deviation $rsd = \sigma/<d>$), on the ripening kinetics. Considering the mass conservation, the PSD function should satisfy [Eq. (3)]

$$\frac{4}{3}\pi\alpha_1 \int_0^\infty f(R,t)R^3 dR = V_0 \quad (3)$$

where V_0 is the initial total volume of supported particles. The particle number $N(t)$ can be obtained via [Eq. (4)]

$$N(t) = \int_0^\infty f(R,t)dR \quad (4)$$

whether the particle of interest grows or shrinks is determined by its curvature radius R larger or smaller than the so-called critical curvature radius R^*. Here, the particle at the critical radius R^* represents a particle whose net flux of the monomer attachment and detachment is zero. Under the mean-field approximation, it is determined by corresponding PSD function.

Under given initial PSD $f(R, t)$, volume V_0 and particle number N, we solve numerically the rate equations for each particles included in PSD and calculate their time evolutions. To do so, the corresponding R^* and proper time step at any given $f(R, t)$ should be decided. Then the change of R for each particle is calculated, and this produces a new PSD, from which corresponding average size, dispersion, particle number and new R^* is derived for next time step. For R^*, there is analytic formula available under the interface or diffusion control limit.[4c, 23] Otherwise, one has to determine R^* numerically, and a bisection algorithm under the constrain of mass conservation is adopted here. To determine the proper time step, we note that for slow process typically happened for large activation energy and average size, and/or at low temperature, larger time step could be used to save the time. Otherwise, smaller time step should be used to maintain the accuracy. Accordingly, an adaptive time-step algorithm is implemented.

For supported particles with narrower PSD or equivalently here higher monodispersity, the difference between R for each particle involved and R^* becomes smaller. Note that for a given particle, there is equilibrium concentration of monomer in far field. As expected, the gradient difference of the far-field monomer concentration between different particles in narrower PSD would be lower, and the driving force for the monomer transportation from the smaller particles toward the larger ones decreases, and so for the ripening rate. For ideal monodispersity, all particles have exactly the same chemical potential, there will be no gradient difference of the monomers between supported particles, and the ripening rate becomes zero.[12]

Acknowledgements

Conflict of interest

The authors declare no conflict of interest.

Keywords: aggregation · computational chemistry · crystal engineering · kinetics · supported particles

[1] a) M. Valden, X. Lai, D. W. Goodman, *Science* **1998**, *281*, 1647–1650; b) I. Lee, F. Delbecq, R. Morales, M. A. Albiter, F. Zaera, *Nat. Mater.* **2009**, *8*, 132–138; c) W. Zhu, R. Michalsky, O. Metin, H. Lv, S. Guo, C. J. Wright, X. Sun, A. A. Peterson, S. Sun, *J. Am. Chem. Soc.* **2013**, *135*, 16833–16836; d) X. F. Yang, A. Q. Wang, B. T. Qiao, J. Li, J. Y. Liu, T. Zhang, *Acc. Chem. Res.* **2013**, *46*, 1740–1748.

[2] T. W. Hansen, A. T. Delariva, S. R. Challa, A. K. Datye, *Acc. Chem. Res.* **2013**, *46*, 1720–1730.

[3] a) D. Kandel, *Phys. Rev. Lett.* **1997**, *79*, 4238–4241; b) M. José-Yacamán, C. Gutierrez-Wing, M. Miki, D. Q. Yang, K. N. Piyakis, E. Sacher, *J. Phys. Chem. B* **2005**, *109*, 9703–9711; c) G. Palasantzas, T. Vystavel, S. A. Koch, J. T. M. De Hosson, *J. Appl. Phys.* **2006**, *99*, 024307–5.

[4] a) P. Wynblatt, N. A. Gjostein, *Acta Metal.* **1976**, *24*, 1165–1174; b) S. C. Parker, C. T. Campbell, *Phys. Rev. B* **2007**, *75*, 035430–15; c) L. R. Houk, S. R. Challa, B. Grayson, P. Fanson, A. K. Datye, *Langmuir* **2009**, *25*, 11225–11227; d) S. R. Challa, A. T. Delariva, T. W. Hansen, S. Helveg, J. Sehested, P. L. Hansen, F. Garzon, A. K. Datye, *J. Am. Chem. Soc.* **2011**, *133*, 20672–20675; e) S. B. Simonsen, I. Chorkendorff, S. Dahl, M. Skoglundh, J. Sehested, S. Helveg, *J. Catal.* **2011**, *281*, 147–155.

[5] a) Q. Xu, K. C. Kharas, B. J. Croley, A. K. Datye, *ChemCatChem* **2011**, *3*, 1004–1014; b) T. van Haasterecht, M. Swart, K. P. de Jong, J. H. Bitter, *J. Energy Chem.* **2016**, *25*, 289–296; c) K. Yu, D. J. Groom, X. P. Wang, Z. W. Yang, M. Gummalla, S. C. Ball, D. J. Myers, P. J. Ferreira, *Chem. Mater.* **2014**, *26*, 5540–5548.

[6] a) P. Munnik, M. E. Z. Velthoen, P. E. de Jongh, K. P. de Jong, C. J. Gommes, *Angew. Chem. Int. Ed.* **2014**, *53*, 9493–9497; b) S. Bonanni, K. Aït-Mansour, W. Harbich, H. Brune, *J. Am. Chem. Soc.* **2014**, *136*, 8702–8707.

[7] a) R. Zanella, V. Rodríguez-González, Y. Arzola, A. Moreno-Rodriguez, *ACS Catal.* **2012**, *2*, 1–11; b) N. Ta, J. J. Liu, S. Chenna, P. A. Crozier, Y. Li, A. Chen, W. Shen, *J. Am. Chem. Soc.* **2012**, *134*, 20585–20588; c) W. Yan, S. M. Mahurin, Z. Pan, S. H. Overbury, S. Dai, *J. Am. Chem. Soc.* **2005**, *127*, 10480–10481; d) K. Qian, W. Huang, Z. Jiang, H. Sun, *J. Catal.* **2007**, *248*, 137–141; e) S. N. Rashkeev, S. Dai, S. H. Overbury, *J. Phys. Chem. C* **2010**, *114*, 2996–3002; f) P. Lu, C. T. Campbell, Y. Xia, *Nano Lett.* **2013**, *13*, 4957–4962; g) R. van den Berg, T. E. Parmentier, C. F. Elkjaer, C. J. Gommes, J. Sehested, S. Helveg, P. E. de Jongh, K. P. de Jong, *ACS Catal.* **2015**, *5*, 4439–4448; h) I. V. Yentekakis, G. Goula, P. Panagiotopoulou, S. Kampouri, M. J. Taylor, G. Kyriakou, R. M. Lambert, *Appl. Catal. B* **2016**, *192*, 357–364; i) J. Jones, H. Xiong, A. T. DeLaRiva, E. J. Peterson, H. Pham, S. R. Challa, G. Qi, S. Oh, M. H. Wiebenga, X. I. Pereira Hernández, Y. Wang, A. K. Datye, *Science* **2016**, *353*, 150–154.

[8] a) F. Yang, M. S. Chen, D. W. Goodman, *J. Phys. Chem. C* **2009**, *113*, 254–260; b) S. B. Simonsen, I. Chorkendorff, S. Dahl, M. Skoglundh, J. Sehested, S. Helveg, *J. Am. Chem. Soc.* **2010**, *132*, 7968–7975; c) N. Chaâbane, R. Lazzari, J. Jupille, G. Renaud, E. A. Soares, *J. Phys. Chem. C* **2012**, *116*, 23362–23370; d) E. Jang, E.-K. Lim, J. Choi, J. Park, Y.-J. Huh, J.-S. Suh, Y.-M. Huh, S. Haam, *Cryst. Growth Des.* **2012**, *12*, 37–39; e) G. S. Parkinson, Z. Novotny, G. Argentero, M. Schmid, J. Pavelec, R. Kosak, P. Blaha, U. Diebold, *Nat. Mater.* **2013**, *12*, 724–728; f) A. Howard, C. E. J. Mitchell, R. G. Egdell, *Surf. Sci.* **2002**, *515*, L504–L508; g) D. E. Starr, S. K. Shaikhutdinov, H. J. Freund, *Top. Catal.* **2005**, *36*, 33–41; h) T. Schalow, B. Brandt, D. E. Starr, M. Laurin, S. Schauermann, S. K. Shaikhutdinov, J. Libuda, H. J. Freund, *Catal. Lett.* **2006**, *107*, 189–196; i) M. Agnelli, M. Kolb, C. Mirodatos, *J. Catal.* **1994**, *148*, 9–21.

[9] a) S. H. Joo, J. Y. Park, C.-K. Tsung, Y. Yamada, P. Yang, G. A. Somorjai, *Nat. Mater.* **2009**, *8*, 126–131; b) J. Lu, B. Fu, M. C. Kung, G. Xiao, J. W. Elam, H. H. Kung, P. C. Stair, *Science* **2012**, *335*, 1205–1208; c) A. Cao, R. Lu, G. Veser, *Phys. Chem. Chem. Phys.* **2010**, *12*, 13499–13510; d) M. T. Bore, H. N. Pham, E. E. Switzer, T. L. Ward, A. Fukuoka, A. K. Datye, *J. Phys. Chem. B* **2005**, *109*, 2873–2880; e) J. Sun, D. Ma, H. Zhang, X. Liu, X. Han, X. Bao, G. Weinberg, N. Pfänder, D. Su, *J. Am. Chem. Soc.* **2006**, *128*, 15756–15764; f) G. Prieto, J. D. Meeldijk, K. P. de Jong, P. E. de Jongh, *J. Catal.* **2013**, *303*, 31–40; g) G. Prieto, M. Shakeri, K. P. de Jong, P. E. de Jongh, *ACS Nano* **2014**, *8*, 2522–2531; h) F. Behafarid, B. Roldan Cuenya, *Top. Catal.* **2013**, *56*, 1542–1559; i) P. Tabib Zadeh Adibi, V. P. Zhdanov, C. Langhammer, H. Groenbeck, *J. Phys. Chem. C* **2015**, *119*, 989–996; j) G. Prieto, J. Zecevic, H. Friedrich, K. P. de Jong, P. E. de Jongh, *Nat. Mater.* **2013**, *12*, 34–39; k) A. K. Datye, Q. Xu, K. C. Kharas, J. M. McCarty, *Catal. Today* **2006**, *111*, 59–67.

[10] a) A. T. Bell, *Science* **2003**, *299*, 1688–1691; b) A. L. M. da Silva, J. P. den Breejen, L. V. Mattos, J. H. Bitter, K. P. de Jong, F. B. Noronha, *J. Catal.* **2014**, *318*, 67–74.

[11] a) S. Sun, C. B. Murray, D. Weller, L. Folks, A. Moser, *Science* **2000**, *287*, 1989–1992; b) J. Park, J. Joo, S. G. Kwon, Y. Jang, T. Hyeon, *Angew. Chem. Int. Ed.* **2007**, *46*, 4630–4660; c) J.-S. J. a. D.-K. L. Nong-Moon Hwang, *InTechOpen* **2012**, https://doi.org/10.5772/50324.

[12] R. Ouyang, J. X. Liu, W. X. Li, *J. Am. Chem. Soc.* **2013**, *135*, 1760–1771.

[13] K. Wettergren, F. F. Schweinberger, D. Deiana, C. J. Ridge, A. S. Crampton, M. D. Rötzer, T. W. Hansen, V. P. Zhdanov, U. Heiz, C. Langhammer, *Nano Lett.* **2014**, *14*, 5803–5809.

[14] V. P. Zhdanov, F. F. Schweinberger, U. Heiz, C. Langhammer, *Chem. Phys. Lett.* **2015**, *631*, 21–25.

[15] S. Zhang, M. Cargnello, W. Cai, C. Murray, G. W. Graham, X. Pan, *J. Catal.* **2016**, *337*, 240–247 .

[16] S. L. Hu, W. X. Li, *ChemNanoMat* **2018**, https://doi.org/10.1002/cnma.201800052.

[17] S. L. Hu, R. Ouyang, W. X. Li, *J. Energ. Chem.* **2018**, https://doi.org/10.1016/j.jechem.2018.03.023.

[18] a) S. Abbet, K. Judai, L. Klinger, U. Heiz, *Pure Appl. Chem.* **2002**, *74*, 1527–1535; b) R. Popescu, R. Schneider, D. Gerthsen, A. Bottcher, D. Loffler, P. Weis, M. M. Kappes, *Surf. Sci.* **2009**, *603*, 3119–3125.

[19] a) D. S. Sidhaye, B. L. V. Prasad, *New J. Chem.* **2011**, *35*, 755–763; b) D.-K. Lee, S.-I. Park, J. K. Lee, N.-M. Hwang, *Acta Mater.* **2007**, *55*, 5281–5288; c) R. Shankar, B. Bin Wu, T. P. Bigioni, *J. Phys. Chem. C* **2010**, *114*, 15916–15923; d) Y. Yang, X. Z. Gong, H. M. Zeng, L. J. Zhang, X. H. Zhang, C. Zou, S. M. Huang, *J. Phys. Chem. C* **2010**, *114*, 256–264; e) P. Sahu, B. L. V. Prasad, *Chem. Phys. Lett.* **2012**, *525–526*, 101–104; f) P. Sahu, B. L. V. Prasad, *Nanoscale* **2013**, *5*, 1768–1771.

[20] V. Buriakov, A. Goriely, *EPL (Europhysics Letters)* **2017**, *119*, 50001–p6.

[21] C. T. Campbell, S. C. Parker, D. E. Starr, *Science* **2002**, *298*, 811–814.

[22] a) J. A. Farmer, C. T. Campbell, *Science* **2010**, *329*, 933–936; b) S. C. Parker, C. T. Campbell, *Top. Catal.* **2007**, *44*, 3–13; c) S. L. Hemmingson, C. T. Campbell, *ACS Nano* **2017**, *11*, 1196–1203.

[23] F. Behafarid, B. Roldan Cuenya, *Surf. Sci.* **2012**, *606*, 908–918.